Reactive Uptake of Nitric Acid onto Sodium Chloride Aerosols Across a Wide Range of Relative Humidities

Thomas D. Saul, Michael P. Tolocka, and Murray V. Johnston*

University of Delaware, Department of Chemistry and Biochemistry, Newark, Delaware 19716

Received: January 30, 2006; In Final Form: April 18, 2006

Reactive uptake coefficients for nitric acid onto size-selected (d_{ve} = 102 and 233 nm) sodium chloride aerosols are determined for relative humidities (RH) between 85% and 10%. Both pure sodium chloride and sodium chloride mixed with magnesium chloride ($X_{Mg/Na}$ = 0.114, typical of sea salt) are studied. The aerosol is equilibrated with a carrier gas stream at the desired RH and then mixed with nitric acid vapor at a concentration of 60 ppb in a laminar flow tube reactor. At the end of the reactor, the particle composition is determined in real time with a laser ablation single particle mass spectrometer. For relative humidities above the efflorescence relative humidity (ERH), the particles exist as liquid droplets and the uptake coefficient ranges from 0.05 at 85% RH to >0.1 near the ERH. The droplet sizes, relative humidity and composition dependencies, are readily predicted by thermodynamics. For relative humidities below the ERH, the particles are nominally "solid" and uptake depends on the amount of surface adsorbed water (SAW). The addition of magnesium chloride to the particle phase (0.114 mole ratio of magnesium to sodium) facilitates uptake by increasing the amount of SAW. In the presence of magnesium chloride, the uptake coefficient remains high (>0.1) down to 10% RH, suggesting that the displacement of chloride by nitrate in fine sea salt particles is efficient over the entire range of conditions in the ambient marine environment. In the marine boundary layer, displacement of chloride by nitrate in fine sea salt particles should be nearly complete within a few hours (faster in polluted areas)—a time scale much shorter than the particle residence time in the atmosphere.

Introduction

Sea salt aerosol is abundant in the marine boundary layer. The chemical composition of freshly formed sea-salt aerosol reflects the water source from which it was generated.[1] Subsequent reactions of these aerosols may sequester reactive nitrogen and affect the ozone budget, especially in the polluted coastal troposphere.[2]

A reaction that has garnered much attention is the uptake of nitric acid onto sodium chloride:

$$NaCl(s,l) + HNO_3(g) \rightarrow NaNO_3(s,l) + HCl(g)$$

Most studies of this reaction have been performed with solid-phase NaCl particles, below the deliquescence relative humidity (DRH) if the bulk solid is initially prepared, or the efflorescence relative humidity (ERH) if liquid droplets are initially prepared, at 75% and 45%, respectively.[3−9] Davies and Cox[5] and Ghosal and Hemminger[10] have studied the reactive uptake onto solid NaCl as a function of relative humidity (RH) below the DRH. The results have helped confirm the hypothesis that surface adsorbed water (SAW) plays an important role for reactivity,[4,11−13] even though the particles are nominally "solid".

Only two studies have examined reactive uptake above the DRH/ERH where the aerosol exists as liquid droplets. Abbatt and Warshewsky[14] measured the uptake for a polydisperse sodium chloride aerosol (RH = 75 ± 3%) with a number median diameter of 3 μm. In this work, nitric acid vapor was the limiting reactant and the decrease in its concentration with reaction time was monitored. The measured uptake coefficient was found to be large (γ_0 > 0.2) and limited by gas-phase diffusion. Tolocka et al.[15] studied this reaction under conditions where the nitric acid vapor was in excess and the particle phase concentrations of nitrate and chloride were measured as a function of reaction time. For droplets (RH ~ 80%) that were approximately 100 and 230 nm in volume equivalent diameter (d_{ve}), uptake was not limited by gas-phase diffusion and the uptake coefficient was found to increase with increasing particle size.

To date, no systematic study of the uptake of nitric acid onto sodium chloride aerosol has been attempted over a broad range of relative humidities above and below the DRH/ERH. In the work described here, uptake is studied between 85 and 10% RH for both pure NaCl and a mixture of NaCl + $MgCl_2$, whose magnesium to sodium mole ratio ($X_{Mg/Na}$ = 0.114) is characteristic of sea salt.[16] The results give insight into the role of particle phase composition on the uptake mechanism and how uptake changes as a function of relative humidity.

Experimental Section

Most aspects of the experimental setup are similar to our previous work.[15] The main components are a flow tube reactor coupled to a real-time laser ablation (193 nm) single particle time-of-flight mass spectrometer operating in negative-ion mode. This instrument determines the chloride-to-nitrate mole ratio in the individual particles exiting the reactor. Pseudo-first-order conditions with respect to nitric acid (60 ± 2 ppb) were maintained in the flow tube reactor by keeping the total salt concentration low. Each experiment employed a different particle number concentration that maximized the mass spectrometer particle hit rate while at the same time kept the maximum amount of nitric acid reacted low (<10%). Relative

* To whom correspondence should be addressed. Telephone: (302) 831-8014. Fax: (302) 831−6335. E-mail: mvj@udel.edu.

10.1021/jp060639a CCC: $33.50
Published on Web 05/25/2006

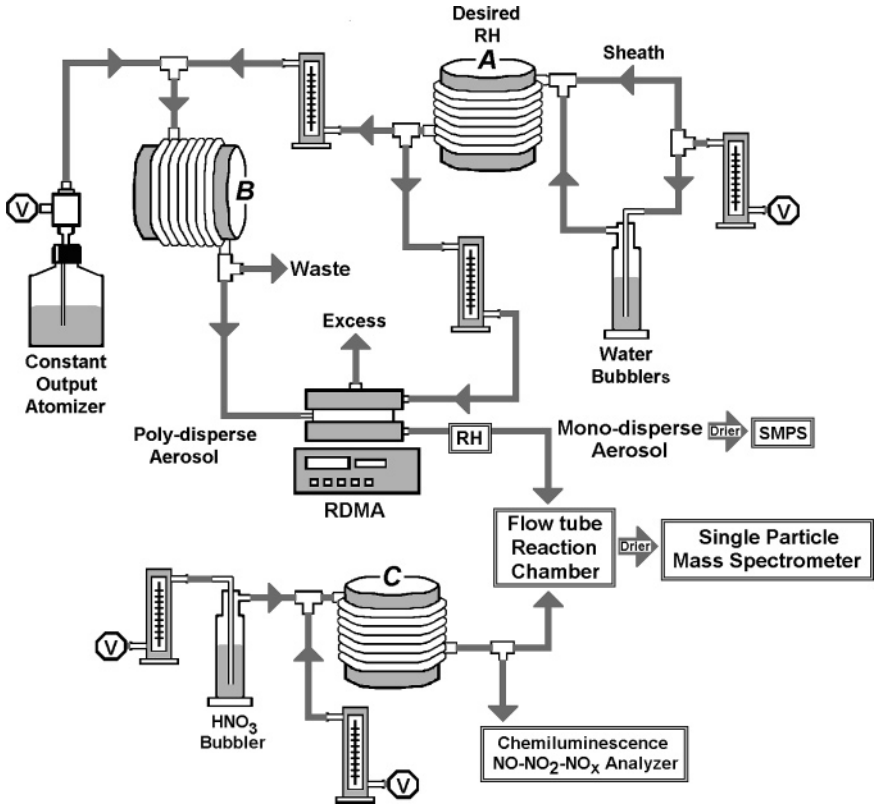

Figure 1. Experimental setup for aerosol generation and size-selection at a specified relative humidity.

to our previous work, both the flow tube reactor and aerosol humidification systems were redesigned. The reactor was partitioned into segmented lengths of interchangeable Quick Flange QF25 (Vacuum Technology, Oak Ridge, TN.) stainless steel (SS) nipples (0.938 in./0.875 in. o.d./i.d.), which were coated with halocarbon wax (Halocarbon Products Corp., River Edge, NJ). PTFE tubing (0.8125 in./0.75 in. o.d./i.d.) was then inserted into the waxed SS QF25 nipples. The halocarbon wax coating served as both a sealant and conduit against surface charging on the PTFE. By combining different lengths of these interiorly lined QF25 nipples, we achieved reaction times of 3.0, 5.0, 7.5 and 10.0 s. The reaction time is given as the total time minus the mixing time (0.5 s or less). The laminar flow velocity in the reactor was 5 cm/s. At the front of the reactor assembly, an interiorly lined QF25 tee housed a central injection tube (for HNO_3 delivery) and the entrance port for the aerosol carrier gas stream. The central injection tube was constructed with SS tubing (0.375 in./0.325 in. o.d./i.d.) that had PTFE tubing (0.3125 in./0.25 in. o.d./i.d.) inserted inside it. Relative to the previous reactor injector, artifacts such as loading and off gassing of adsorbed nitric acid to/from the inner walls were minimized, allowing more precise and accurate control of the gas-phase concentration.

The reactant conditioning systems are shown in Figure 1. Mixing spiral A consists of approximately 15 ft in length of polyethylene tubing (0.25 in./0.17 in. o.d./i.d.), firmly wrapped around a cylindrical wire frame. Saturated water vapor is produced by bubbling air through two wash bottles filled with deionized water. A Drierite scrubber dries sheath air. The separate flows of dry air and humidified air sent into mixing spiral (A) are regulated with Accucal flow meters (models 6541-1215 & -1225, Gilmont Instruments, Barrington, IL). The humidified air is then split two directions. One leads to the particle-free flow inlet of a home-built radial differential mobility analyzer (RDMA).[17] The other serves as the total dilution air supplied to mixing spiral B. A mass flow controller (model FMA-A2408, Omega, Stamford, CT) regulates the excess humidified air of the RDMA. Mixing spiral B consists of approximately 15 ft in length of Tygon tubing (0.375 in./0.25 in. o.d./i.d.), also firmly wrapped around a cylindrical wire frame. A polydisperse droplet spray is created with a constant output atomizer (Model 3076, TSI Inc., St. Paul, MN) and directed into mixing spiral B. The residence time for the aerosol in mixing spiral B is ~6 s. The aerosol is assumed to have the same molar ratio of salts as the nebulized solution. Droplets equilibrate with the ambient surroundings in mixing spiral B and water condenses or evaporates as necessary to maintain thermodynamic equilibrium.[18,19] At a set potential and flow rate, the RDMA size selects aerosol of a specific mobility diameter (d_m). For relative humidities above the ERH, the salt concentration in the droplets is greatest just above the ERH and decreases with increasing ambient RH. For relative humidities below the ERH, water associated with the aerosol is assumed to be surface adsorbed (SAW) or water molecules trapped within the crystal lattice. The RH of the monodisperse aerosol exiting the RDMA ($\sigma_g < 1.3$) is measured with a NIST-traceable hygrometer (Model 11-661-7B, Control Co., Friendswood, TX) and flows into the outer tube of the reactor. The concentration of nitric acid vapor is regulated in mixing spiral C, which is made of approximately 15 ft of PTFE tubing (0.25 in./0.17 in. o.d./i.d.) wrapped around a cylindrical wire frame. Sheath air is gently bubbled (<50 mL/min) through 15.8 M HNO_3, diluted by a second flow of sheath air (>5 L/min) and sent into mixing spiral C. The concentration of the nitric acid vapor is then measured in real time with a chemiluminescence $NO-NO_2-NO_x$ Analyzer (Thermo Environmental model 42C, Franklin, MA) and directed into the central injection tube of the reactor.

The aerosol size distribution is measured with a scanning mobility particle sizer (SMPS) that consists of a differential mobility analyzer (DMA) and a condensation particle counter

(CPC) (model 3936, TSI Inc., St. Paul, MN). After exiting the RDMA, but before being sampled into the SMPS, the monodisperse aerosol stream is dried by passage through a Nafion diffusion dryer (model MD-110-12S-4, Perma Pure Inc., Toms River, NJ). Dry sodium chloride particles are cubic in shape, which affects the mobility diameter measurement by the SMPS. To compensate, the measured mobility diameters are converted to volume equivalent diameters (d_{ve}).[20] For solid NaCl, a dynamic shape correction factor (χ) of 0.96 is used to obtain d_{ve}[21]

$$d_{ve} = (\chi)d_m \quad (1)$$

For solid NaCl−$MgCl_2$ mixed composition particles, it is assumed that the hygroscopicity and/or polycrystallinity induced by the presence of magnesium chloride provides a more spherical shape after drying.[22,23] Thus, the mobility diameter and the volume equivalent diameter are assumed to be the same (i.e., $\chi = 1$). This assumption is consistent with experimental measurements.

At each RH, the mode (by number) mobility diameter from each monodisperse particle profile is used to estimate d_{ve} as described above. The values of d_{ve} are then used to calculate an effective aerosol volume (V_{eff}) before drying (V_{wet}) and after drying (V_{dry}) from the relationship:

$$V_{eff} = \frac{\pi}{6}(d_{ve})^3 \quad (2)$$

For the V_{dry} measurements, dry (RH < 5%) sheath air is utilized in the SMPS. For the V_{wet} measurements, the monodisperse aerosol exiting the RDMA bypasses the Nafion diffusion dryer and the same relative humidity of the sheath air in the RDMA is sent into the SMPS. The aerosol chloride concentration, [Cl^-], in the wet aerosol is then obtained:

$$[Cl^-] = \frac{V_{dry}\rho_{eff}(X_{Cl})}{V_{wet}(MW)} \quad (3)$$

where X_{Cl} is the mole fraction chloride (determined by single particle mass spectrometry) in the particle after reaction with HNO_3, ρ_{eff} is the effective aerosol density (g/cm^3) and MW is the formula weight (g/mol). For NaCl, $\rho_{NaCl} = 2.16$ and $MW_{NaCl} = 58.44$. The same quantities for the mixed aerosol ($MgCl_2$/NaCl) were estimated from the magnesium to sodium mole fraction:

$$MW_{MgCl_2/NaCl} = (0.886MW_{NaCl}) + (0.114MW_{MgCl_2}) \quad (4)$$

$$\rho_{MgCl_2/NaCl} = \frac{(\rho_{NaCl}\rho_{MgCl_2})(0.886MW_{NaCl} + 0.114MW_{MgCl_2})}{[(0.886MW_{NaCl}\rho_{MgCl_2}) + (0.114MW_{MgCl_2}\rho_{NaCl})]} \quad (5)$$

where $\rho_{MgCl_2} = 2.32$ g/cm^3 and $MW_{MgCl_2} = 95.21$ g/mol. The resulting values are $\rho_{MgCl_2/NaCl} = 2.19$ g/cm^3 and $MW_{MgCl_2/NaCl} = 62.64$ g/mol.

Figure 2 shows how the aerosol chloride concentration changes with relative humidity for both compositions. As the RH decreases toward the ERH, the chloride concentration increases. The ERH of pure NaCl as determined from Figure 2, 45 ± 1% RH, agrees well with literature values.[18,24,29] The salt concentrations above the ERH are qualitatively similar to those reported by Cohen et al.,[19] but a quantitative comparison would require accurate values for the droplet densities. The addition of magnesium chloride to the sodium chloride aerosol decreases the ERH to 40 ± 2% and the phase transition is more gradual. Particulate phase water is observed with the SMPS down to 30% RH. At the lower RH's (30−10%), surface water exists on the particles but requires a more sensitive measurement technique than SMPS to be detected.[21] The smallest change measurable with the SMPS, a 2 nm change for a $d_{ve} \sim 100$ nm particle, corresponds to approximately a 6% change in particle volume or 10 monolayers if evenly distributed over the particle surface. At each individual RH, the chloride concentration is slightly greater for $MgCl_2$/NaCl than for pure NaCl, as expected from the stoichiometry of magnesium vs sodium salts. The total number of chloride atoms per particle ($Cl_{tot.}$) prior to reaction is given by

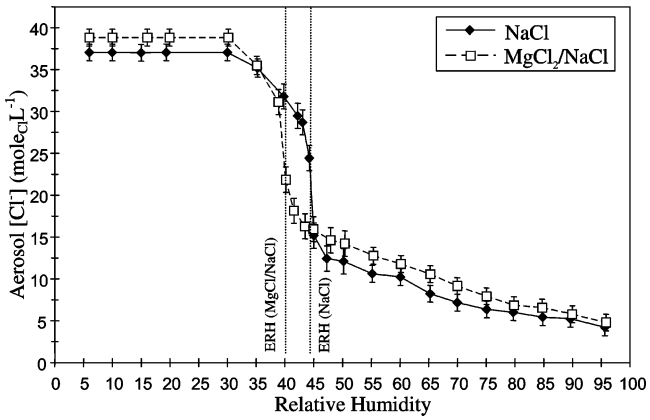

Figure 2. Aerosol chloride concentration vs relative humidity for "pure" NaCl and a Mg/Na mole ratio of 0.114.

$$Cl_{tot.} = \frac{V_{dry}\rho_{eff}N_A}{(MW)_{eff}} \quad (6)$$

where N_A is Avogadro's number. Values of $Cl_{tot.}$ for 102 nm (d_{ve}) particles are given in Table 1 for each RH.

The laser ablation single-particle mass spectrometer is described in detail elsewhere.[25] A detected single-particle negative-ion mass spectrum is the result of one particle/droplet interacting with HNO_3 vapor in the flow tube reactor. Each individual spectrum is integrated to quantify the associated signal corresponding to chloride (sum of 35 and 37 *m*/*z*) and nitrate (sum of 46 and 62 *m*/*z*). A relative ion response (RIR) is obtained for each integrated spectrum by dividing the chloride signal by the total signal (sum of chloride and nitrate). To improve precision, 100 RIRs from 100 individual spectra are averaged for each experiment. The mole fraction chloride (X_{Cl}) in the particles is obtained from a plot of RIR versus mole fraction for particle standards having known compositions.[15]

Results and Discussion

Figures 3 (NaCl) and 4 ($MgCl_2$/NaCl) show how the mole fraction chloride (X_{Cl}) in the particles changes with relative humidity and exposure time. Each point in these figures is the average of many experiments: for droplets, 12 experiments or 1200 single particle spectra; for "dry" particles, 8 experiments or 800 single particle spectra; over 1 million total single particle spectra between Figures 3 and 4. The average mole fractions and standard deviations are shown for each combination of RH and exposure time. For all RH values, X_{Cl} decreases with increasing exposure time and there is a clear break point at the ERH. When Figures 3 and 4 are compared, the decrease in X_{Cl} below the ERH is noticeably greater for $MgCl_2$/NaCl than for

TABLE 1: Initial Number of Chloride Atoms, $Cl_{tot.}$, in a Single 102 nm Diameter Particle vs Relative Humidity

	% RH													
	10	20	30	35	40	45	50	55	60	65	70	75	80	85
NaCl[a]	12.3	12.3	12.0	11.7	10.6	5.04	4.02	3.58	3.40	2.74	2.38	2.11	2.00	1.81
$MgCl_2$/NaCl[a,b]	13.0	13.0	13.0	11.6	7.28	5.33	4.76	4.27	3.94	3.54	3.06	2.65	2.29	2.20

[a] All values are $\times 10^6$. [b] Mg/Na mole ratio = 0.114.

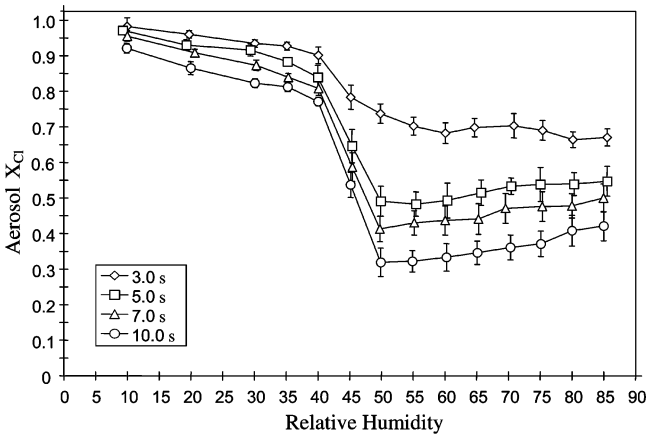

Figure 3. Mole fraction of chloride (X_{Cl}) remaining in NaCl particles vs relative humidity and exposure time (d_{ve} = 102 nm; $[HNO_3]$ = 60 ppb).

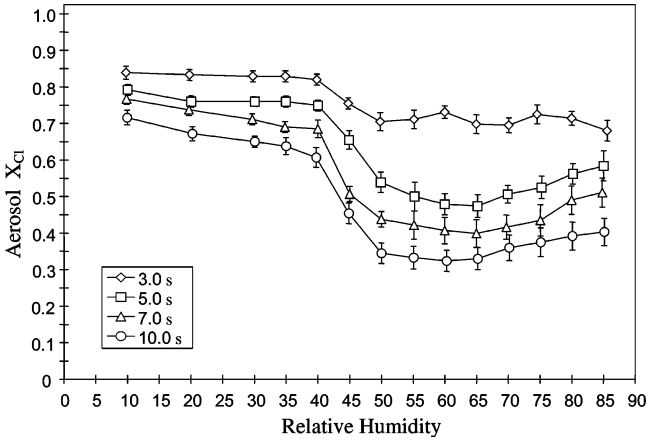

Figure 4. Mole fraction of chloride (X_{Cl}) remaining in $MgCl_2$/NaCl (Mg/Na = 0.114) particles vs relative humidity and exposure time (d_{ve} = 102 nm; $[HNO_3]$ = 60 ppb).

NaCl. The greater reactivity of $MgCl_2$/NaCl is consistent with the hygroscopic character of magnesium salts that facilitates uptake by increasing SAW.

As in our previous work,[15] a pseudo-first-order rate expression is used to analyze the data:

$$\frac{d[Cl^-]}{dt} = -k_I[Cl^-] \tag{7}$$

where $k_I = k_{II}[HNO_3]$. When integrated, eq 7 gives

$$\frac{[Cl^-]_t}{[Cl^-]_0} = e^{-k_I t} = X_{Cl,t} \tag{8}$$

Pseudo-first-order rate constants (k_I) at each RH were obtained by a nonlinear least-squares minimization between the measured (Figures 3 and 4) and calculated (using eq 8) values of $X_{Cl,t}$. Nonlinear minimization allows the uncertainties associated with each $X_{Cl,t}$ measurement to be directly incorporated into the fit

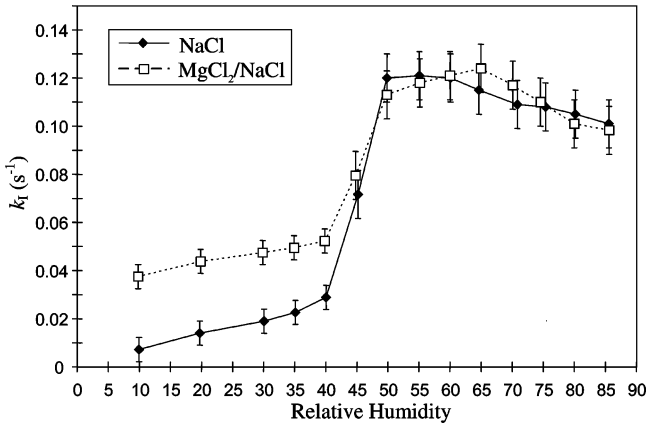

Figure 5. Pseudo-first-order rate constant (k_I, s^{-1}) vs relative humidity for NaCl (◆) and $MgCl_2$/NaCl (□) particles.

and it provides a more equal weighting of the various measurements when determining k_I. Figure 5 shows the calculated rate constants (for d_{ve} = 102 nm) as a function of relative humidity for both NaCl and $MgCl_2$/NaCl. At RH values above the ERH, HNO_3 interacts with highly concentrated aerosol droplets and the mole fraction of chloride changes quickly with exposure time. The values of the rate constants increase slightly as the RH is decreased toward the ERH and are similar for both NaCl and $MgCl_2$/NaCl. At RH values below the ERH, HNO_3 interacts with nominally solid particles in the presence of surface adsorbed water (SAW). The rate constants for $MgCl_2$/NaCl are about a factor of 3 greater than those of pure NaCl, and the rate constants for both compositions decrease with decreasing RH.

The initial reactive uptake coefficient (γ_0) of nitric acid onto NaCl and $MgCl_2$/NaCl is given by

$$\gamma_0 = \frac{k_I Cl_{tot.}}{\frac{\pi}{4} d_{ve}^2 v[HNO_3]} = \frac{2 d_{ve} k_I [Cl^-]}{3v[HNO_3]} \tag{9}$$

where k_I is obtained from Figure 5, $Cl_{tot.}$ is obtained from Table 1, v is the average molecular speed, and d_{ve} is the volume equivalent diameter. Equation 9 assumes spherical particles, which is not necessarily the case below the ERH. However, use of the volume equivalent diameter (d_{ve}) should minimize any shape-related discrepancies. Figure 6 shows the values of γ_0 at each RH and for each composition. The uncertainties for γ_0 in Figure 6 are much greater than those for k_I in Figure 5 because they include uncertainties in the particle diameter.

Uptake Mechanism at RH above the ERH. In our previous work with NaCl droplets at RH = 80%, reactive uptake of HNO_3 was found to be first order in both the gas-phase HNO_3 and condensed-phase Cl^- concentrations, and the uptake coefficient was found to increase linearly with particle size over the size range studied.[15] These results suggested that HNO_3 uptake is limited by the formation of molecular HCl throughout the droplet which is then released into the gas phase. Other common uptake mechanisms are inconsistent with the observed reactant

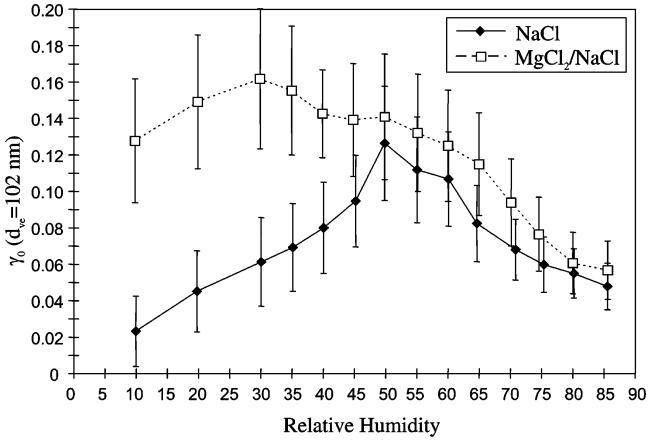

Figure 6. Initial uptake coefficient (γ_0) vs relative humidity for NaCl (◆) and $MgCl_2$/NaCl (□) particles.

concentration and particle size dependencies. In particular, diffusion in either the gas or condensed phase does not affect HNO_3 uptake by particles in this size range.[15]

The results presented here for two particle compositions over a wide range of RH are consistent with these conclusions. First, the rate coefficients (Figure 5) for RH values above the ERH are the same within experimental error for $MgCl_2$/NaCl and pure NaCl, and both suggest a slight increase with decreasing RH between 85% and 50%, although the increase is within experimental error. The similarity between $MgCl_2$/NaCl and NaCl is expected, as the identity of the counterion should not affect the HCl dissociation equilibrium. An increasing rate coefficient with decreasing RH could be caused by changes in ion activity that push the acid dissociation equilibrium toward molecular HCl as the aerosol chloride concentration increases. Second, the uptake coefficients (Figure 6) increase with decreasing RH and uptake by $MgCl_2$/NaCl particles is systematically greater than that by pure NaCl. Both of these dependencies mirror changes in the aerosol chloride concentration with RH and composition (Figure 2)—approximately a 3-fold increase in both concentration and uptake coefficient when going from 85% to 50% RH, and systematically higher values of concentration and uptake coefficient for $MgCl_2$/NaCl vs NaCl. A linear dependence of uptake coefficient on chloride concentration is expected on the basis of eq 9.

Further confirmation that uptake is limited by reaction throughout the particle rather than diffusion to/from the interface or reaction at the interface is gained through the particle size dependence. In the present work, a larger particle size (d_{ve} = 233 nm) was size selected and reacted under the same pseudo-first-order conditions. Two representative relative humidities were chosen for reaction with the d_{ve} = 233 nm aerosols: 60% RH for droplets and RH 20% for "solid" particles. Figure 7 shows the X_{Cl} remaining in the particle phase after reaction in the NaCl and $MgCl_2$/NaCl d_{ve} = 233 nm aerosols. For comparison, the data from the initial study (d_{ve} = 102 nm) at same RH's are superimposed. At 60% RH for both NaCl and $MgCl_2$/NaCl, the mole fraction chloride (X_{Cl}) remaining after reaction is greater for the d_{ve} ~233 nm droplets than for the d_{ve} = 102 nm droplets. Corresponding values for $Cl_{tot.}$, k_I and γ_0 are compared for the two droplet sizes in Table 2 (pure NaCl) and Table 3 ($MgCl_2$/NaCl).

Tables 2 and 3 show for both compositions at 60% RH that the measured rate constants (k_I) decrease, while the initial uptake coefficients and $Cl_{tot.}$ increase with increasing droplet size. The magnitudes of these changes are generally within experimental error of the ratio of the two droplet sizes and are independent

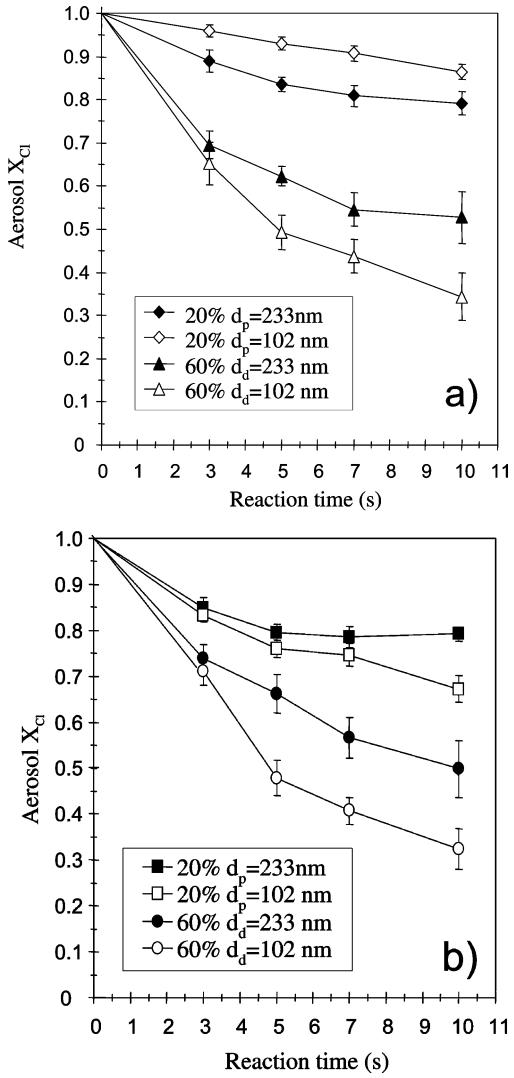

Figure 7. Mole fraction of chloride (X_{Cl}) remaining in (a) NaCl and (b) $MgCl_2$/NaCl particles vs reaction time for 20% and 60% relative humidity.

TABLE 2: Particle Size Dependence of Kinetic Parameters for "Pure" NaCl[a]

	RH 20%		RH 60%	
	d_p = 102 nm	d_p = 233 nm	d_d = 102 nm	d_d = 233 nm
Cl_{tot}	1.2×10^7	1.4×10^8	3.4×10^6	4.5×10^7
k_I	0.014 ± 0.005	0.032 ± 0.006	0.120 ± 0.010	0.081 ± 0.006
γ_0	0.045 ± 0.025	0.24 ± 0.04	0.11 ± 0.025	0.18 ± 0.05

[a] Units: $Cl_{tot.}$ (atoms), k_I (s^{-1}).

TABLE 3: Particle Size Dependence of Kinetic Parameters for a $MgCl_2$/NaCl Mole Ratio of 0.114[a]

	RH 20%		RH 60%	
	d_p = 102 nm	d_p = 233 nm	d_d =102 nm nm	d_d = 233 nm
$Cl_{tot.}$	1.3×10^7	1.6×10^8	3.9×10^6	5.3×10^7
k_I	0.044 ± 0.005	0.039 ± 0.004	0.120 ± 0.011	0.075 ± 0.004
γ_0	0.12 ± 0.04	0.31 ± 0.04	0.10 ± 0.03	0.20 ± 0.05

[a] Units: $Cl_{tot.}$ (atoms), k_I (s^{-1}).

of the presence of $MgCl_2$ in the droplets. Again, these results are consistent with our previous work at 80% RH and are expected if uptake is limited by the formation of molecular HCl in the condensed phase. It should be noted, however, that the magnitudes of the uptake coefficients in the present work are larger than previously reported.[15] The reason for this discrepancy

is a systematic error in the gas-phase HNO_3 measurement in the previous work that was eliminated in the present work through a redesign of the flow tube reactor (see Experimental Section).

Uptake Mechanism at RH below the ERH. Previous studies of nitric acid uptake onto NaCl at relative humidities below the ERH/DRH have shown that uptake is driven by surface adsorbed water (SAW) and that the uptake coefficient varies over a wide range, from 10^{-4} to 10^{-2} depending upon the amount of SAW present.[5,7−10,14,26,29] The experiments described here are somewhat different from previous work in that specific particle sizes are selected and the RH is regulated and systematically varied. Single particle mass spectrometry analyzes the total chemical content (in this work, X_{Cl}) and will not distinguish reaction on the aerosol surface from its bulk.[23] In contrast to RH values above the ERH, the rate and uptake coefficients for $d_{ve} = 102$ nm particles in Figures 5 and 6 show large differences between the two compositions at RH values below the ERH.

For both compositions, the rate coefficients decrease quickly with decreasing RH around the ERH and then continue to decrease with decreasing RH below the ERH (Figure 5). Below the ERH, the rate coefficients for $MgCl_2$/NaCl are greater than those for pure NaCl, which reflects the higher water content and reactivity of the mixed composition particles. The uptake coefficients (Figure 6) show very different behavior at RH values below the ERH. Pure NaCl particles show a monotonic decrease in the uptake coefficient as the RH and amount of SAW decrease. The $MgCl_2$/NaCl composition shows a more complex behavior. Below the ERH, the uptake coefficient continues to increase with decreasing RH, reaching a maximum at 30% RH, and then decreases slightly with further decrease in RH.

Below the ERH, uptake is influenced by both the amount of SAW and the chloride concentration in the SAW. For the $MgCl_2$/NaCl composition, the amount of SAW is large and measurable with the SMPS down to 30% RH. If the chloride concentration within the SAW continues to increase with decreasing RH below the ERH, as it does within the droplet phase above the ERH, then the uptake coefficient will continue to increase. This provides a reasonable explanation for the increase in γ_0 down to 30% RH. Below 30% RH, the amount of SAW becomes small enough that the rate of chloride displacement can no longer be maintained. In principle, it is possible for nominally solid particles that the reaction "shuts off" prior to completion. In other words, complete displacement of chloride by nitrate at RH values below the ERH may not be achieved owing to a buildup of immobile $NaNO_3$ at the particle surface or slow chloride replenishment in SAW. However, the data in Figures 3, 4 and 7 give no indication of such a limitation for fine particles.

Tables 2 and 3 show how the rate and uptake coefficients at 20% RH change with particle size. For pure NaCl, the uptake coefficient of 233 nm particles is almost an order of magnitude larger than that for 102 nm particles. This increase cannot be rationalized simply on the basis of particle surface-to-volume ratio, and strongly suggests that the amount of SAW increases significantly with increasing particle size. If the 102 nm particles resemble single crystals, flat terrace sites with minimal SAW may initially exist on the particle surface, limiting uptake.[10] As the particle size increases to 233 nm, a polycrystalline particle may exist with more structural imperfections available to host SAW sites. In contrast, for $MgCl_2$/NaCl particles at 20% RH, the magnitude of the increase in uptake coefficient is the same within experimental error as the increase in particle size. This dependence is similar to that observed for droplets at RH values above the ERH. Although the composition, RH and size dependencies at RH values below the ERH can be rationalized, they are not easily predicted as there is currently no model for quantitative prediction of SAW.

Other Influences on Uptake. In addition to chemical reaction, other processes that can affect uptake include gas-phase diffusion, mass accommodation at the gas−particle interface and solubility/diffusion in the particle phase. For the particle sizes studied in this work, the effect of gas-phase diffusion is very small and does not affect the measured uptake coefficients.[15] Indeed, the limited influence of gas-phase diffusion is a significant advantage of these experiments as it allows other factors influencing uptake to be investigated. The accommodation (sticking) coefficient for HNO_3 (α_{HNO_3}) on the particles studied here is large due to its high solubility. For example, α_{HNO_3} has been measured as 0.19 ± 0.02 for micrometer size water droplets at ~90% RH.[27] The measured uptake coefficients in other experiments have been assumed to be equivalent to α_{HNO_3}: >0.2 for ~3 μm unbuffered NaCl droplets at ~75% RH,[14] and as large as 0.50 ± 0.20 for ~70 nm synthetic sea salt at ~55% RH.[28] For both the NaCl and $MgCl_2$/NaCl compositions studied in this work, a logarithmic dependence of the chloride loss with time was observed. If the measured uptake were solely due to α_{HNO_3}, the constant collision rate of HNO_3 with the aerosol would produce a linear decrease in X_{Cl} with increasing reaction time. The observed logarithmic dependence of X_{Cl} with time suggests that $\alpha_{HNO_3} > 0.15$.

The influence of HNO_3 solubility on uptake depends on reaction time and the condensed phase diffusion coefficient. At $t = 0$, solubility has no effect on uptake. For the maximum exposure times in this study (10 s), the resistance due to HNO_3 solubility ($1/\Gamma_{sol}$) is estimated to be <2.3 and is not a major contributor to uptake ($1/\gamma_0 > 6$). However, the calculation of $1/\Gamma_{sol}$ assumes an aqueous phase with a typical liquid phase diffusion coefficient and therefore applies directly only to droplets (i.e., at RH values >ERH). For "solid" particles, the importance of Γ_{sol} to uptake is difficult to assess owing to the morphological differences in the crystalline structures at SAW sites. It has been shown that surface water enhances ion mobility and the ability to open up fresh NaCl reactive sites.[10] Hoffman et al.[3] suggest that the regeneration of chloride in these SAW sites is fast compared to reaction. If we assume these conditions, dissolution on the particle surface will be independent of time and the effect of Γ_{sol} will also be negligible for "solid" particles.

Conclusions. The measurements reported here constitute the first systematic study of reactive uptake across a wide range of relative humidities. For relative humidities above the ERH, the reactive uptake coefficient of nitric acid onto sodium chloride ranges from 0.05 at 85% RH to >0.1 near the ERH. The droplet size and relative humidity dependencies are readily predicted by thermodynamics and independent of the presence of another cation (magnesium). For relative humidities below the ERH, the reactive uptake coefficient depends on chemical composition. Magnesium chloride, at a molar level typically found in sea salt, facilitates nitric acid uptake by increasing the amount of surface adsorbed water. In the presence of magnesium chloride, the uptake coefficient remains high (>0.1) down to 10% RH suggesting that the displacement of chloride by nitrate in fine sea salt particles is efficient over the entire range of conditions in the ambient marine environment.

Efficient displacement of chloride by nitrate in fine particles is an important aspect of the marine boundary layer. Although coarse ($d_p > 0.6$ μm) sea-salt particles constitute most of the

aerosol mass, particles smaller than 0.6 μm account for about 90% of the total number of particles in the marine atmosphere.[30] The chemical composition of these fine particles are often mixtures soluble and insoluble organic carbons, non-sea-salt sulfate and sea salt.[31] Coastal breaking waves produce an abundance of fine particles, from as small as 0.01 μm up to a number peak near 0.03−0.40 μm, which are primarily composed of sea salt.[32] Depending on meteorological conditions, the residence time for fine particles is on the order of days, compared to hours for coarse particles.[33] Given the uptake coefficients determined in this work and an average nitric acid concentration of 160 ppt,[18] the displacement of chloride by nitrate in fine particles should be nearly complete within a few hours—a time scale much shorter than their residence time in the atmosphere. Displacement will be even faster in the polluted marine environment where the nitric acid concentration is much higher. The uptake coefficients for the "solid" particles reported here are 1−3 orders of magnitude greater than those obtained from previous studies.[2,4−5,10−13,24] The larger values reported here reflect the significant role that particulate water contributes to reactivity for relative humidities and particle sizes relevant to the marine boundary layer.

Acknowledgment. This research was supported by the National Science Foundation under grant number CHE-0517972. We thank Prof. Douglas P. Ridge of the Department of Chemistry and Biochemistry, University of Delaware, for helpful discussions on kinetics.

References and Notes

(1) Raes, F.; Van Dingenen, R.; Vignati, E.; Wilson, J.; Putaud, J.-P.; Seinfeld, J. H.; Adams, P. *Atmos. Environ.* **2000**, *34*, 4215−4240.
(2) Finlayson-Pitts, B. J.; Hemminger, J. C. *J. Phys. Chem. A* **2000**, *104*, 11463−11477.
(3) Hoffman, R. C.; Kaleuati, A.; Finlayson-Pitts, B. J. *J. Phys. Chem. A* **2003**, *107*, 7818−7826.
(4) Finlayson-Pitts, B. J. *Chem. Rev.* **2003**, *103*, 4801−4822.
(5) Davies, J. A.; Cox, R. A. *J. Phys. Chem. A* **1998**, *102*, 7631−7642.
(6) Sporleder, D.; Ewing, G. E. *J. Phys. Chem. A* **2001**, *105*, 1838−1846.
(7) Leu, M.-T.; Timonen, R. S.; Keysey, L. F.; Yung, Y. L. *J. Phys. Chem.* **1995**, *99*, 13203−13212.
(8) ten Brink, H. M. *J. Aerosol Sci.* **1998**, *29*, 57−64.
(9) Beichert, P.; Finlayson-Pitts, B. J. *J. Phys. Chem.* **1996**, *100*, 15218−15228.
(10) Ghosal, S.; Hemminger, J. C. *J. Phys. Chem. A* **1999**, *103*, 4777−4781.
(11) Peters, S. J.; Ewing, G. E. *J. Phys. Chem. B* **1997**, *101*, 10880−10886.
(12) Peters, S. J.; Ewing, G. E. *Langmuir* **1997**, *13*, 6345−6348.
(13) Allen, H. C.; Laux, J. M.; Vogt, R.; Finlayson-Pitts, B. J.; Hemminger, J. C. *J. Phys. Chem.* **1996**, *100*, 6371−6375.
(14) Abbatt, J. P. D.; Waschewsky, G. C. G. *J. Phys. Chem. A* **1998**, *102*, 3719−3725.
(15) Tolocka, M. P.; Saul, T. D.; Johnston, M. V. *J. Phys. Chem. A* **2004**, *108*, 2659−2665.
(16) Lide, D. R. *Handbook of Chemistry and Physics*, 72nd ed.; CRC Press Inc.: Boca Raton, FL, 1991−1992; p 14-10.
(17) Zhang, S.-H.; Akutus, Y.; Russell, L.; Flagan, R. C. *Aerosol Sci. Technol*. **1995**, *23*, 357−372.
(18) Finlayson-Pitts, B. J.; Pitts, J. N., Jr. *Chemistry of the Upper and Lower Atmosphere. Theory, Experiments and Applications*; Academic Press: San Diego, CA, 2000.
(19) Cohen, M. D.; Flagan R. C.; Seinfeld, J. H. *J. Phys. Chem.* **1987**, *91*, 4563−4574.
(20) DeCarlo, P. F.; Slowik, J. G.; Worsnop, D. R.; Davidovits, P.; Jimenez, J. L. *Aerosol Sci. Technol*. **2004**, *38*, 1185−1205.
(21) Romakkaniemi, S.; Hämeri, K.; Väkevä, M.; Laaksonen, A. *J. Phys. Chem. A* **2001**, *105*, 8183−8188.
(22) Laskin, A.; Iedema. M. J.; Cowin, J. P. *Environ. Sci. Technol*. **2002**, *36*, 4948−4955.
(23) Krueger, B. J.; Grassian, V. H.; Iedema, M. J.; Cowin, J. P.; Laskin, A. *Anal. Chem.* **2003**, *75*, 5170−5179.
(24) Tang, I. N.; Munkelwitz, H. R. *Atmos. Environ.* **1993**, *27A*, 467−473.
(25) Kane, D. B.; Johnston, M. V. *Environ. Sci. Technol.* **2000**, *34*, 4887−4893.
(26) Rossi, M. J. *Chem. Rev.* **2003**, *103*, 4823−4882.
(27) Van Doren, J. M.; Watson, L. R.; Davidovits, P.; Worsnop, A. P.; Zahniserr, M. S.; Kolb, C. E. *J. Phys. Chem.* **1990**, *94*, 3265−3269.
(28) Guimbaud, C.; Arens, F.; Gutzwiller, L.; Gäggeler, H. W.; Ammann, M. *Atmos. Chem. Phys. Discuss.* **2002**, *2*, 739−763.
(29) Wise, M. E.; Biskos, G.; Martin, S. T.; Russell, L. M.; Buseck, P. R. *Aerosol Sci. Technol*. **2005**, *39*, 849−856.
(30) Pandis, S. N.; Wexler, A. S.; J. H. Seinfeld *J. Phys. Chem.* **1995**, *99*, 9646−9659.
(31) O'Dowd, C. D.; Facchini, M. C.; Cavalli, F.; Ceburnis, D.; Mircea, M.; Decesari, S.; Fuzzi, S.; Yoon, Y. J.; Putaud, J.-P. *Nature* **2004**, *431*, 676−680.
(32) Clark, A.; Kapustin, V.; Howell, S.; Moore, K.; Lienert, B.; Masonis, S.; Anderson, T.; Covert, D. *J. Atmos. Oceanic Technol*. **2003**, *20*, 1362−1374.
(33) Gong, S. L.; Barrie, L. A.; Blanchet, J.-P. *J. Geophys. Res.* **1997**, *102*, 3805−3818.